International Journal of Fluid Machinery and Systems
Vol. 4, No. 4, October-December 2011

DOI: http://dx.doi.org/10.5293/IJFMS.2011.4.4.360
ISSN (Online): 1882-9554

Original Paper

Prediction of Cascade Performance of Circular-Arc Blades with CFD

Masami Suzuki[1], Toshiaki Setoguchi[2] and Kenji Kaneko[3]

[1]Department of Mechanical Engineering, Graduate School of Engineering, The University of Tokyo
7-3-1 Hongo, Bunkyo-ku, Tokyo, 113-8656 Japan, wells@mech.t.u-tokyo.ac.jp
[2]Institute of Ocean Energy, Saga University
1 Honjo-machi, Saga-shi, Saga, 840-8502, Japan, setoguchi@me.saga-u.ac.jp
[3]Department of Mechanical Engineering, Saga University
1 Honjo-machi, Saga-shi, Saga, 840-8502, Japan

Abstract

Thin circular-arc blade is often used as a guide vane, a deflecting vane, or a rotating blade of low pressure axial-flow turbomachine because of its easy manufacture. Ordinary design of the blade elements of these machines is done by use of the carpet diagrams for a cascade of circular-arc blades. However, the application of the carpet diagrams is limited to relatively low cambered blade operating under optimum inlet flow conditions. In order to extend the applicable range, additional design data is necessary. Computational fluid dynamics (CFD) is a promising method to get these data. In this paper, two-dimensonal cascade performances of circular-arc blade are widely analyzed with CFD. The results have been compared with the results of experiment and potential theory, and useful information has been obtained. Turning angle and total pressure loss coefficients are satisfactorily predicted for lowly cambered blade. For high camber angle of 67°, the CFD results agree with experiment for the angle of attack less than that for shockless inlet condition.

Keywords: Circular-arc blades, Cascade, Guide Vane, Potential Flow, CFD

1. Introduction

Computer environments are commonly equipped in these days, so CFD has become useful and important design tool of turbomachine. On the other, experimentally obtained design data has higher reliability compared with CFD. However, it needs a great deal of experimental work. Therefore the practical and reliable CFD tool is expected. The carpet diagram also exists for the design of circular-arc blade cascades and the cascade data are on a level that it can be fully applicable to a standard design. However, individual experimental data are required in order to grasp the cascade characteristics for the flow condition out of the applicable range of the carpet diagram, i.e. large inlet angle, large turning angle or off design condition. Potential flow calculation result can well predict the accelerated cascade flow since it does not cause the strong adverse pressure gradient which causes the separation on blade. However, the decelerated cascade flow generates the separation even around the shockless entry conditions as the camber angle of blade increases. Therefore notable difference between experiment and a potential flow occurs in case of the decelerated cascade flow. Special type of turbomachine like natural energy converter always suffers intense fluctuation of input energy, so the operation condition drops into off design range frequently. Therefore it is required to grasp the flow characteristics over the wide range including off design condition. Guide vane attached in the Wells turbine for wave power generation [1] is mentioned to one of such the objects. The Wells turbine is special turbine which can rotate always one-way in the oscillating air flow generated by up-and-down motion of a wave. The turbine has simple structure symmetrical with the surface of rotation. For this reason the guide vane profiles built-in at up- and down-stream sides of the rotor necessarily becomes symmetrical, and both edges of the blade become also to a leading edge or a trailing edge alternatively. Therefore, the simple blade of circular-arc profile is adopted to the guide vane of Wells turbine. The aim of this work is to provide the design data of circular-arc blade cascade which is fit to such a special operation by means of CFD, verifying the calculation accuracy. This work is also endeavoring approach to an experiment based on the new knowledge.

Received December 25 2009; revised June 24 2011; accepted for publication August 13 2011: Review conducted by Prof. Seung Jin Song. (Paper number O09054)
Corresponding author: Masami Suzuki, Assistant Professor, wells@mech.t.u-tokyo.ac.jp

2. Circular-Arc Blade Cascade

Figure 1 shows the circular-arc blade cascade. The calculations is performed under conditions that camber angles are θ =13.73°, 31.88°, 49.63° and 66.8°, solidities are $\sigma=l/s$=0.666, 1.0 and 1.333, considering the experiment which was carried out by Ikui, et al. [2]. Reynolds number is Re=1.9×10^5 based on the inlet velocity V_1 and the chord length l as representative velocity and length. The experiment is performed by changing the stagger angle γ (or angle of attack α_1) around the shockless entry condition, for the constant inlet angle β_1.

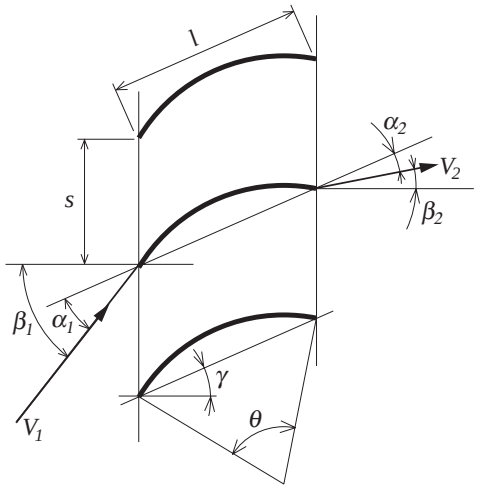

Fig. 1 Parameters for two-dimensional cascade of circular-arc blade

3. Numerical Method

An in-house code [3] used to a viscous calculation is an incompressible finite volume Navier-Stokes solver which is developed originally. The solver is based on structured grids and the use of curve-linear boundary fitted coordinates. The code uses a collocated variable arrangement (Perić et al., [4]) and the Rhie and Chow interpolation method [5] is used to avoid odd-even pressure decoupling. The SIMPLE algorithm (Patankar, [6]) is used for pressure-velocity coupling. The convection term is calculated using a third-order quadratic upwind interpolation (QUICK) scheme (Leonard, [7]) and the other terms in space are calculated using a second-order difference schemes. It is well known that sophisticated turbulence models do not always produce better results than the very simple models. For practical applications that are computationally expensive it is often wiser to use a simple approach. Therefore the proven and computationally efficient Launder-Sharma low-Reynolds-number k-ε turbulence model [8] and Kato and Launder k-ε turbulence model [9], are used in this report. Unsteady computations are made with three-point backward differencing for the time derivative, which is a second-order-accurate implicit algorithm, stable for large time steps and thereby decreases the computational time.

3.1 Grid System

Figure 2 shows the H-type grid topology around 2-D circular-arc blade cascade which is arranging 50 points in the pitchwise direction and 120 points in the streamwise which consist of 80 points along the blade surface and 20 points in each up- and down-stream side of blade. The grid spacing normal to the blade surface is 1.0×10^{-4} along the entire blade surface. The streamwise grid spacing at the leading and the trailing edge is 1.0×10^{-3} with maximum values at mid-chord reaching approximately 3.0×10^{-2}. The non-dimensional time step based on the inlet velocity and the chord length is 1.3×10^{-3} for the unsteady computations. It is considered that the influence of blade thickness can be ignored by the reason why the thickness of the circular-arc blades used for the experiment is very thin such as 1.2% chord length. Therefore the blade thickness is set to zero in numerical computation and thereby the grid distortion at the leading edge is reduced and the single grid generation is made easy. The interface between blades is making the grid in agreement along the periodic boundary so that a conservation rule is satisfied, while the orthogonality of the grid is reduced at the interface.

3.2 Boundary Condition

The boundary conditions are set up classifying into the inlet, the outlet, the interface between cascade blades and the blade surface.

Inlet boundary

The inlet flow are uniform and the turbulent kinetic energy, k, and the dissipation, ε, are specified at the inlet boundary. The turbulent kinetic energy, k, and the dissipation, ε are calculated by 1% in turbulence intensity and the eddy viscosity which is 10% in molecular viscosity. The boundary conditions for the pressure are prescribed using a Neumann condition (zero gradient).

Outlet boundary

The outlet boundary conditions for the flow and the turbulence properties (k and ε) are given as a convective boundary condition, and the pressure are prescribed using a Neumann condition (zero gradient).

Periodic boundary

The periodic boundary conditions are given for all variables along the interface between cascade blades except for the blade surface.

Wall (blade surface) boundary

No-slip conditions are implemented at the blade surface, with flow velocity vectors u and v set to zero. The turbulence properties are specified to be $k=\varepsilon=0$. Pressure gradients in the wall normal direction are set to zero. The y^+ is kept less than 1 for the first grid point from the blade surface.

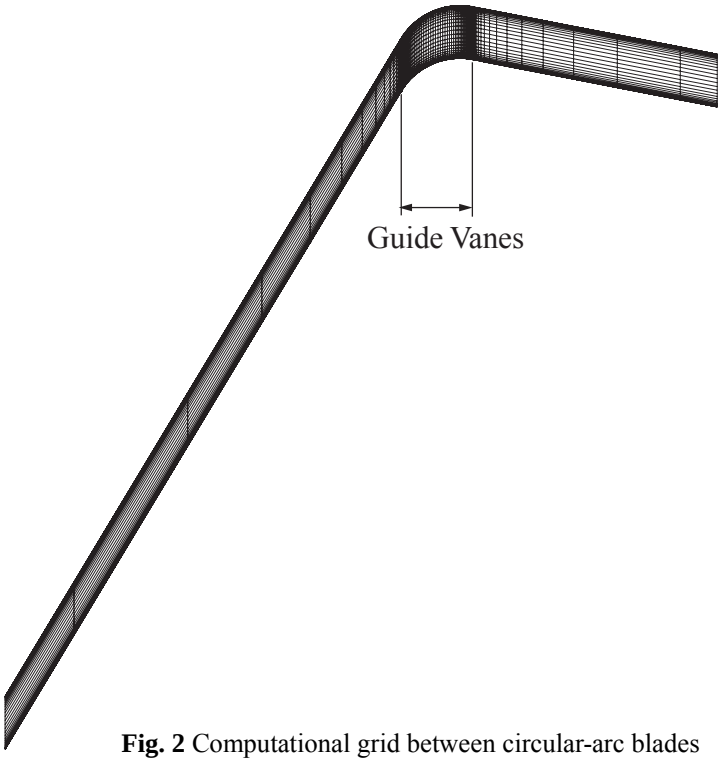

Fig. 2 Computational grid between circular-arc blades

4. Comparison between CFD and Experimental Result

Figure 3 shows the turning angles $\Delta\beta(=\beta_1-\beta_2)$ and the total pressure loss coefficients ζ_p of the circular-arc blades cascade with the camber angles less than θ =50°. It is the results for three camber angles, θ =13.7°, 31.88°, 49.63° at the inlet angle β_1=40° and the solidity σ = 1.0. The dashed line expresses the potential flow and, the calculation results of Navier-Stokes equation are shown in the solid line, and the open circles express the experimental results. The long dashed short dashed line in the figure shows the shockless angle of attack calculated by the potential flow which is solved by the singular point method [1] which arranges vortexes on the blade surface. In the turning angle below 50°, the results of Navier-Stokes equation shown by the solid lines agree well with the experimental results of open circles, and the difference decreases with decreasing camber angle. Particularly the difference in the turning angle is less than 0.5° around the shockless angle of attack shown by the long dashed short dashed line. For the small camber angle, such as θ =13.7°, the potential flow is also well in agreement with the results of Navier-Stokes equation and the experiment. However, with increasing camber angle, such as θ =31.88°, 49.63°, the difference between the potential flow and the experiment result appears notably, because the larger separation is generated on the blade. The total pressure loss coefficient, ζ_p is expressed as following equation:

$$\zeta_p = \frac{(p_1 + 0.5\rho V_1^2) - (p_2 + 0.5\rho V_2^2)}{0.5\rho V_1^2} \qquad (1)$$

which is the differential total pressure between the inlet and outlet divided by the dynamic pressure of inlet velocity, where p_1, p_2 and ρ are the static pressure at inlet, the static pressure at outlet, and the air density respectively. The calculation results of the total pressure loss coefficient, ζ_p is presumed less than the experimental results about 0.02. However the relative variation of ζ_p against the angle of attack agrees well with both viscous calculation and the experimental results, and the minimum value appears around the shockless angle of attack similarly to the experiment. As a result, the viscous calculation is accurate enough for practical use to determine a design angle of attack within the camber angles in Fig.3.

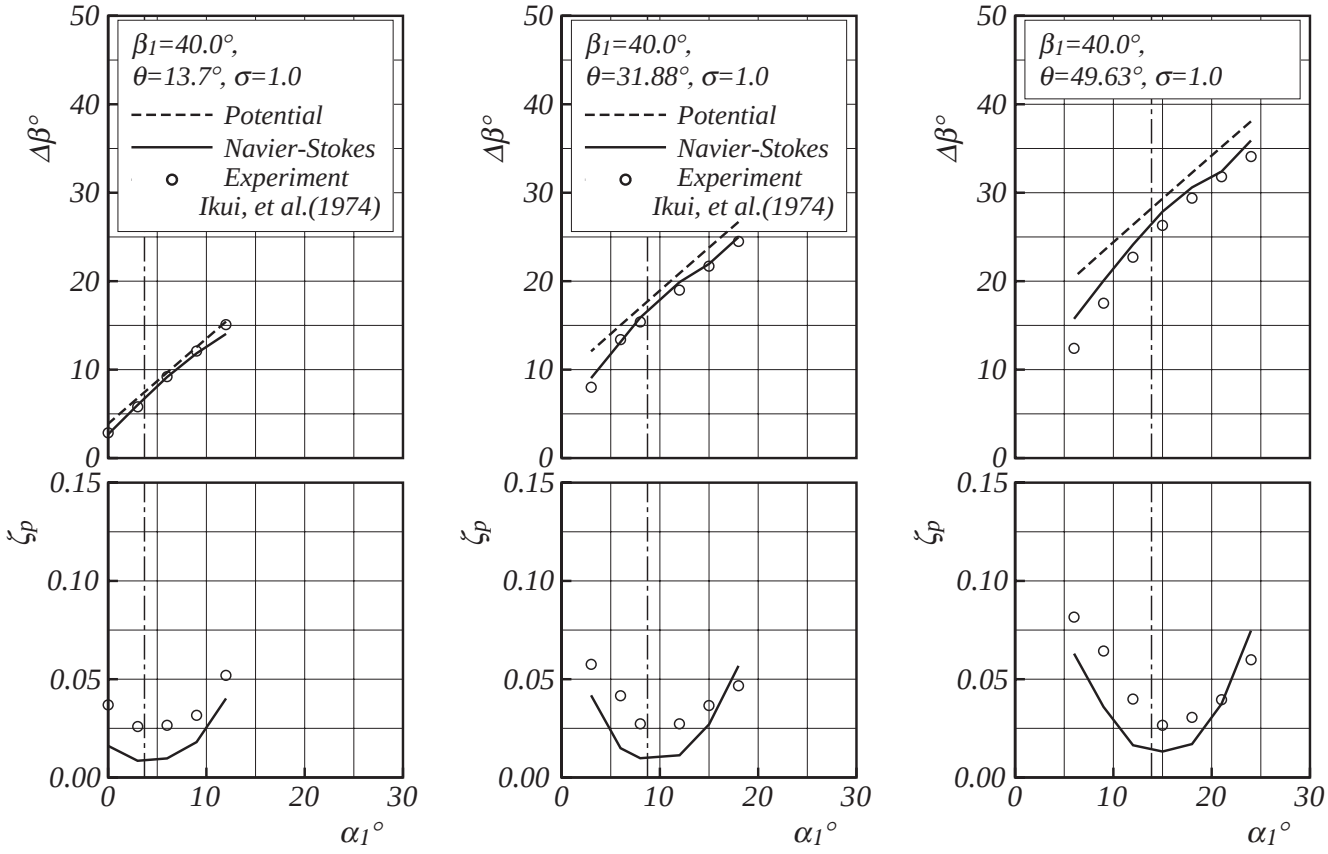

Fig. 3 Cascade performance of circular-arc blades with camber angle less than 50°: turning angle (top) and total pressure loss coefficient (bottom)

Figure 4 shows the tuning angle, $\Delta\beta$ and the total pressure loss coefficient, ζ_p for the large camber angle, θ =66.8°, and inlet angle, β_1=40°, which expresses the effect of the solidities, σ =0.666, 1.0 and 1.333 respectively. The turning angle, $\Delta\beta$ for σ =0.666 and 1.0 agrees well between the viscous calculation and the experiment in the region less than the shockless angle of attack indicated by the long dashed short dashed line. Above the shockless angle of attack, the experimental results show tendency of stall, on the other hand the viscous calculations show that the turning angle increases as increasing angle of attack, that is, tendency of no-stall. Furthermore, for high solidity, σ =1.333, the tuning angles of experiment over angle of attack α_1=18° are lower than the results of the viscous calculation even below the shockless angle of attack. The relative variation of the total pressure loss coefficient agrees well between the viscous calculation and the experimental results at the smaller angle of attack than shockless entry such as Fig.3, and it becomes the minimum value around shockless entry. Complete agreement was observed at particular solidity σ =0.666. Since the turning angle shows the completely different tendency between the viscous calculation and the experimental results in larger angle of attack than the shockless entry, the total pressure loss coefficient has also notable difference between both. In consequence an important subject rises from the above result. It is the point that the tendency of turning angle differs greatly at the angle of attack over the shockless entry when the camber angle is large as θ =66.8°. In order to make clear the reason why these differences have arisen, the pressure distributions on the blade and the flow fields in the blade passage are investigated.

Figures 5~7 show the pressure distributions on the blade and the streamlines for σ =1.0 in solidity. The flow is unsteady basically and the separation region is transferring. Therefore the instantaneous pressure coefficients have large fluctuation. The flow changes along irregular time interval. Figs. 5~7 also show the flow fields from the smallest angle of attack, α_1=6° near the shockless entry, to the largest angle of attack, α_1=24°. Moreover, the pressure distribution over the blade passage is also expressed with gray scale together with the streamline, where the deep black indicates high pressure and the white indicates low pressure. The pressure distributions on the blade show the potential flow results (dashed line), the instantaneous value (solid line) of viscous calculation, and the time average value (open circle) of viscous calculation (NS). At α_1=6° which is smaller angle of attack than the shockless entry (Fig.5), leading edge stall occurs generating large separation over the underside surface (pressure side surface). At α_1=18° which is the angle of attack near the shockless entry, the small separation appears near the leading edge on the underside surface of blade; however the pressure distributions are in agreement between the viscous calculation and the potential calculation. At α_1=24° which is larger angle of attack than the shockless entry (Fig. 7), although the slight trailing edge separation

appears at the upper side surface, the pressure distributions of viscous calculation and potential calculation are in agreement. On the other hand, the turning angle in the experimental results of α_1=24° shown in the center figure (σ =1.0) of Fig. 4 becomes very low caused by stalling. It is resumed that the large separation is produced at the upper side surface (suction side surface) in the experiment unlike the calculation. Usually, the calculation using the turbulent flow model tends to make easy transition to turbulence as compared with an experiment, and tends to restrict the large separation produced by an adverse pressure gradient. The prediction of the overestimate turning angle and the underestimate total pressure coefficient may be caused at the angle of attack over the shockless entry by the influence. For this reason, the calculation without a turbulence model by which the growth of a separation is accelerated more was also carried out, and the influence on the turning angle and the total pressure loss coefficient over the angle of attack for the shockless entry was also considered. However, investigating the results in the left figure of Fig. 4 (σ =0.666), following conclusions are obtained. Since even in the calculation with the turbulence model clear transition is not attained because of the low Reynolds number, the remarkable difference between with and without turbulence model is not found out for the turning angle and the total pressure loss coefficient. Therefore the further examination is also required for the factors (e.g. the generation process of the separation) which cause the difference between the calculation and the experimental results. The difference between the viscous calculation and the experimental results shown in this session is the interesting and important problem for the cascade blade which requires a large turning angle. We should perform the improvement of a numerical computation code, and also clarify an application limit through various cascade calculation and experimental results including the calculation and the experiment error in the future. In addition, in the experiment a 3-hole Pitot tube is traversed at one chord length downstream from the trailing edge of the blade, and the turning angle and the total pressure loss coefficient are space averaged over 1-pitch. On the other hand, in the numerical computation, calculation of a turning angle and total pressure loss coefficient is performed at the inlet and the outlet boundary of the 5-chord length upstream from the leading edge and the 3-chord length downstream from the trailing edge which are in the normal direction of cascade. The influence of these traverse position is investigated by the numerical computation result, and it is confirmed that the average of incident angle, the outlet angle and the total pressure do not change at upstream and downstream position more than 1-chord length of blade. Even downstream, the outlet angle error is less than 0.2° and that of the non-dimensional total pressure is less than 0.002. As mentioned above, the viscous calculations are in agreement with the experimental results except the angle of attack over the shockless entry, and it is confirmed that the 2-dimensionality and measuring accuracy of experiment is also enough.

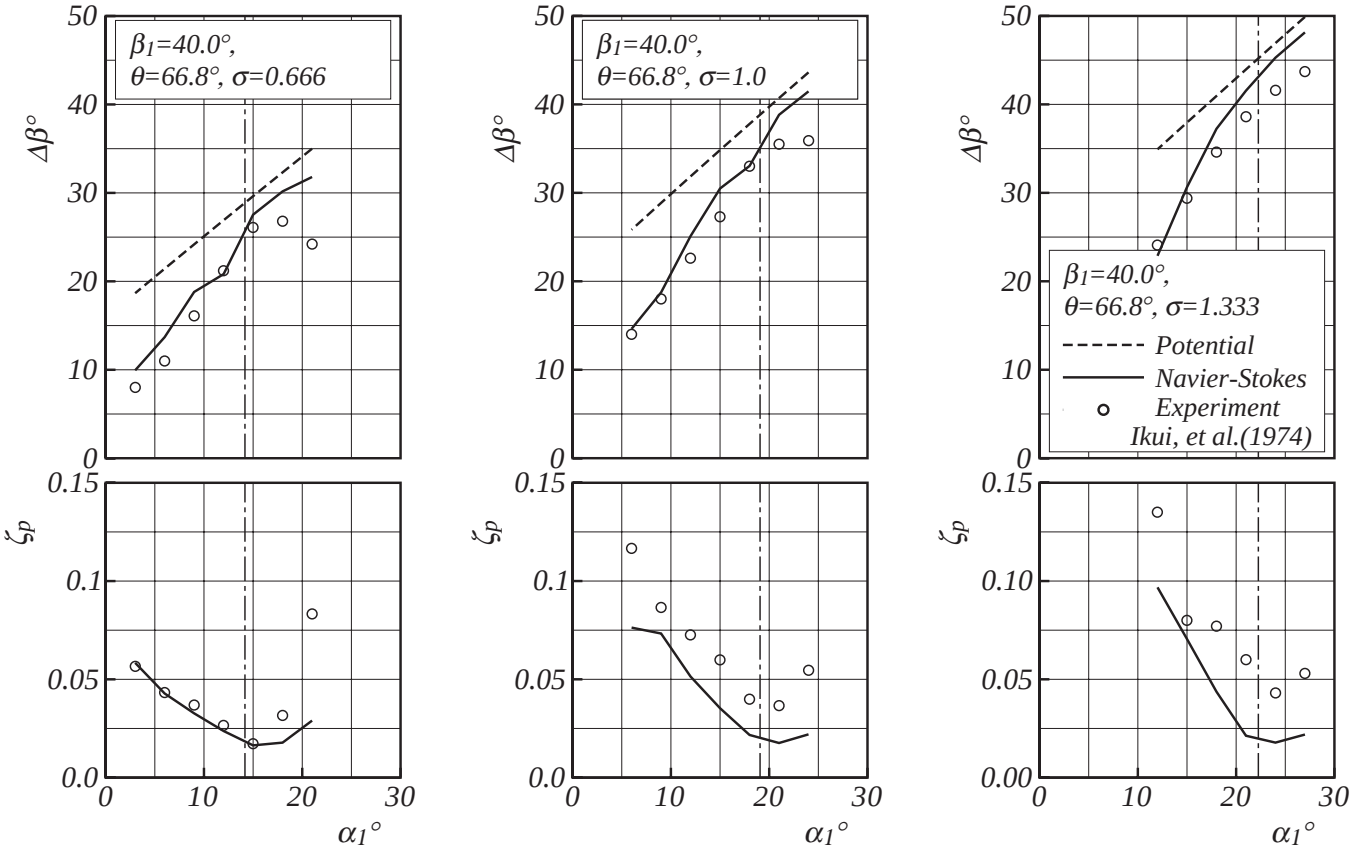

Fig. 4 Cascade performance of circular-arc blades with camber angle θ =66.8°: turning angle (top) and total pressure loss coefficient (bottom)

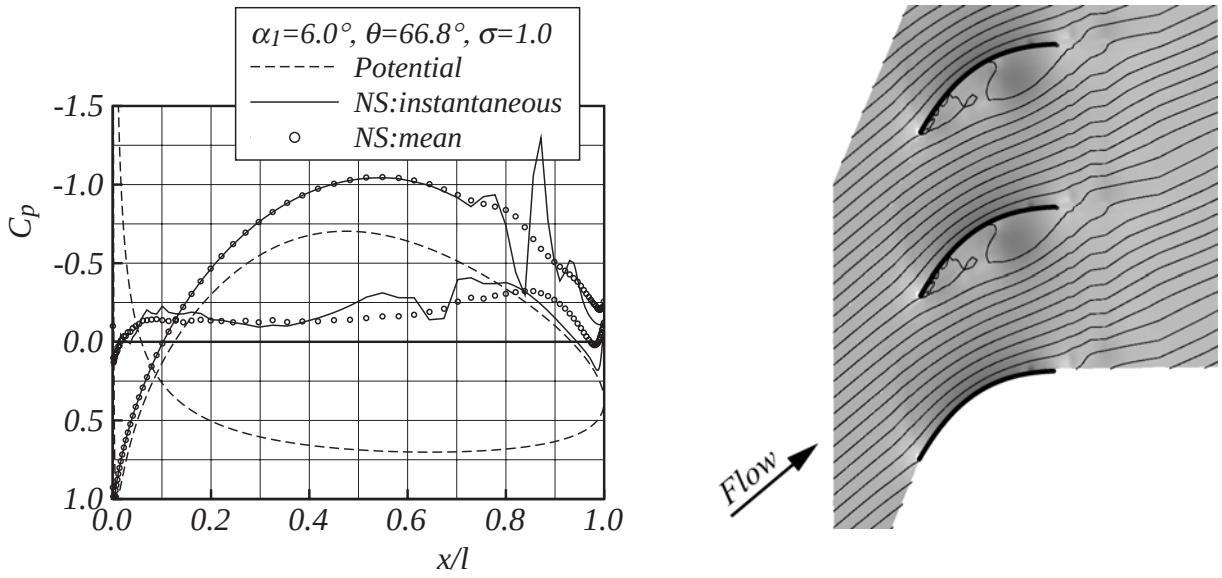

Fig. 5 Pressure distribution at α_1=6.0°

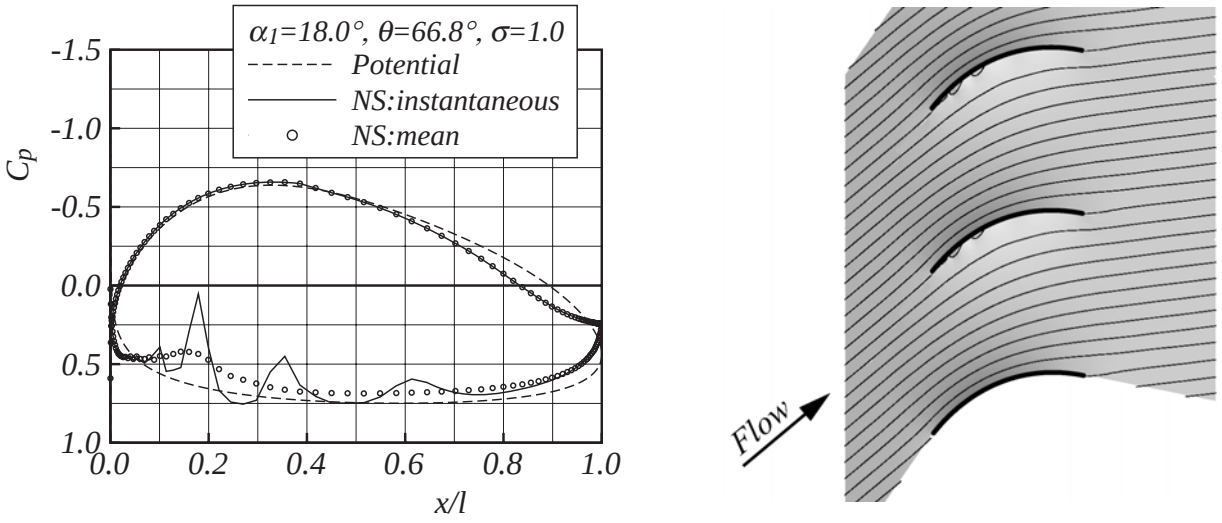

Fig. 6 Pressure distribution at α_1=18.0°

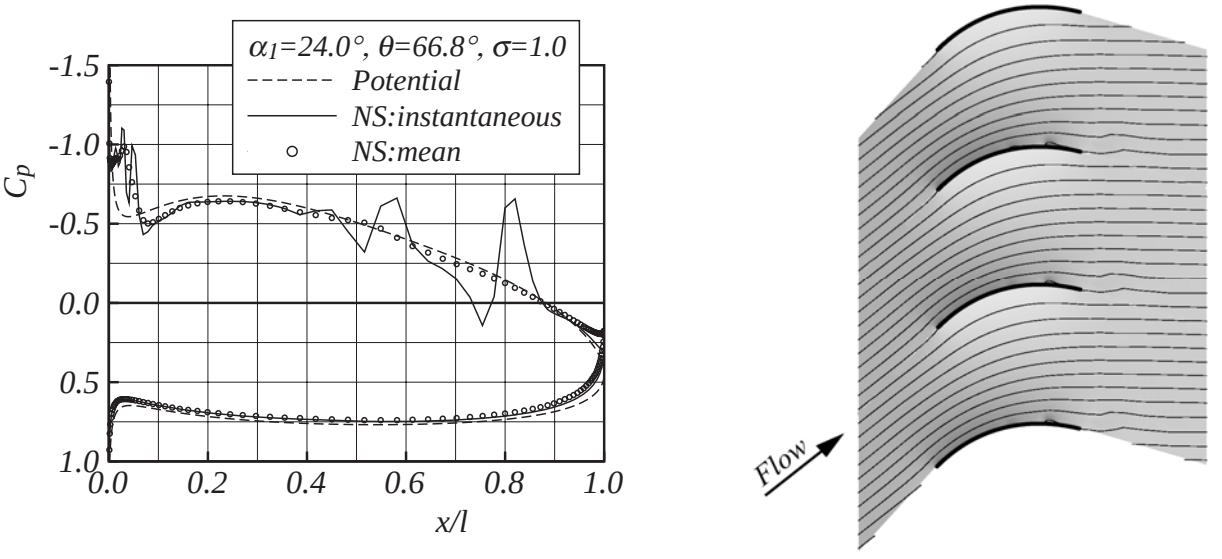

Fig. 7 Pressure distribution at α_1=24.0°

5. Conclusion

Usually, although the reliability of an experiment is considered to be high level as compared with numerical computation, only an experimental result does not secure quantitative absolute accuracy and expresses the relative accuracy which includes an absolute deviation error in each experiment. Good practical use of the computational fluid dynamics is expected also from the viewpoint of validating the deviation error by the difference among the experimental equipments, the experimental methods, and so on. The present study investigates the accuracy of the performance of the circular-arc blade cascade predicted by the computational fluid dynamics to take the practical use of CFD into consideration, and the following results are clarified.

(1) The turning angle is well in agreement between the CFD and the experimental results, and the CFD is sufficiently useful when the camber angle of the circular-arc blade is below 49.63°.
(2) Below the shockless angle of attack, the turning angle is in agreement between the experimental and CFD result, even though the flow is separated at the leading edge on the pressure side surface. Since it is considered that the leading edge separation is fixed at the leading edge independently of the turbulence transition and so on because of the very thin blade. The separation on the suction side surface plays important role over shockless angle of attack, and the high turning angle is produced because the separation region of CFD is appeared small as compared with the experiment.
(3) Although the total pressure loss coefficient predicted by CFD shows smaller value by as much as 0.02 than the experimental result quantitatively, the qualitative tendency of loss coefficient is well similar.

Acknowledgments

The work has been supported in part by the Cooperative Research Program of IOES, Institute of Ocean Energy, Saga University (Accept No.07001D) and the Grant-in-Aid for Scientific Research (C) No.20560742 from Japan Society for the Promotion of Science.

References

[1] Suzuki, M., 2006, “Design Method of Guide Vane for Wells Turbine,” Journal of Thermal Science, Vol. 15, No. 2, pp. 126-131.
[2] Ikui, T., Inoue, M., Kaneko, K., 1971, “Two-Dimensional Cascade Performance of Circular-Arc Blades,” Proceedings of Tokyo Joint International Gas Turbine Conference and Products Show, JSME-9, pp. 57-64.
[3] Suzuki, M., 2006, “Investigation into Accuracy of CFD for Flow around Isolated Airfoil,” Turbomachinary, Vol. 34, No. 6, pp. 366-373 (in Japanese).
[4] Perić, M., Kessier, R., Scheuerer, G., 1988, “Comparison of Finite-Volume Numerical Methods with Staggered and Collocated Grids,” Computers & Fluids, Vol. 16, No. 4, pp. 389-403.
[5] Rhie, C. M. and Chow, W. L., 1983, “Numerical Study of the Turbulent Flow Past an Airfoil with Trailing Edge Separation,” AIAA Journal, Vol. 21, No. 11, pp. 1525-1532.
[6] Patankar, S. V., 1980, “Numerical Heat Transfer and Fluid Flow,” McGraw-Hill, New York.
[7] Leonard, B. P., 1979, “A Stable and Accurate Convective Modelling Procedure Based on Quadratic Upstream Interpolation,” Computer Methods in Applied Mechanics and Engineering, 19, pp. 59-98.
[8] Launder, B.E., Sharma, B.I., 1974, “Application of the Energy-Dissipation Model of Turbulence to the Calculation of Flow near a Spinning Disk,” Letters in Heat Mass Transfer, Vol. 1, pp. 131-138.
[9] Kato, M., Launder, B. E., 1993, “The modeling of turbulent flow around stationary and vibrating square cylinder,” Proceedings of 9th Symposium Turbulent Shear Flows, Kyoto, Paper 10-4.